Numerical Study of the High-Speed Leg of the National Transonic Facility

S. Melissa Rivers
NASA Langley Research Center
Hampton, VA
USA

Sudheer N. Nayani and Ana F. Tinetti
Analytical Services & Materials, Inc.
Hampton, VA
USA

Scott E. Brynildsen
Craig Technologies
Hampton, VA
USA

Ryan J. Ferris
Exa Corporation
Burlington, MA
USA

s.m.rivers@nasa.gov

ABSTRACT

The initial phase of a computational effort to characterize the flow inside the National Transonic Facility is summarized. High-fidelity representations of the "as-built" structures comprising the high-speed leg of the facility were used to obtain solutions for three configurations: empty tunnel, body of revolution installed, and NASA Common Research Model installed. The capabilities of three grid generators (VGRID, Heldenmesh, and PowerFLOW®) and two flow solvers (USM3D and PowerFLOW®) were assessed in the effort. The extreme geometric complexity of the tunnel precluded successful application of VGRID to the generation of a suitable volume mesh. Various aspects of flow solutions at high subsonic Mach numbers are presented and discussed.

1.0 INTRODUCTION

Most wind tunnel facilities in existence were designed using either empirical methods or idealized lumped-parameter models of the tunnel circuit. When the complexity of the tunnel exceeds the limitations of the empirical models, the design process is typically supported with tests of isolated sections of the circuit using small-scale models. If the facility is geometrically complex, or represents a new generation of testing capabilities, numerical simulations of the flow within the circuit can yield better, safer designs and useful information for the improvement of wall corrections in instances when the size of the model taxes existing assumptions.

Numerical simulations of the flow within a wind tunnel facility can provide important benefits when used as an adjunct to experimental testing. The most obvious advantage is the ability to better understand the aerodynamic characteristics of the facility, including the identification of anomalies such as flow nonuniformity or unsteadiness caused by flow separation in the circuit or by wakes emanating from vanes and support structures. The simulations can also help identify areas where unexpected losses occur, provide a better estimate of the aerodynamic loads on the tunnel structure and support hardware, and aid in the design of improvements within the tunnel circuit.

This paper summarizes the initial computational aspect of an ongoing investigation aimed at characterizing the flow within the National Transonic Facility (NTF), located at the NASA Langley Research Center (LaRC). The current numerical effort is limited to the high-speed leg of the facility, comprised of the settling chamber (turbulence control screens not included), 15:1 contraction, transition to test section, test and model support sections, plenum, and high-speed diffuser. All of the important geometric complexities of the facility were considered, including 1) the model mounting system, and 2) the 12 slots and 14 reentry flaps in the ceiling and floor of the test section used to prevent choked flow effects. Other secondary structures, such as the apparatuses that support the plenum and the reentry flap system, and various blockages within the plenum, were included as they affect plenum volume, and thus may modify test section flow entrainment.

A discussion of the entire process of modelling this wind tunnel is given, from the initial laser scans to the development of a volume grid. Preliminary results from transonic flow simulations of the empty tunnel, an installed body of revolution (C4 BoR), and the NASA Common Research Model (CRM) installed in the tunnel are presented and discussed.

2.0 NATIONAL TRANSONIC FACILITY

Plans for the NTF were conceived in the late 1970s as its predecessor, the NASA LaRC 4×4-Foot Supersonic Pressure Tunnel, was being decommissioned [1]. Parts of the older facility, such as drive motors, cooling towers, and other support structures, were incorporated into the NTF design. The new tunnel would serve all national commercial, military, and scientific requirements for transonic flow investigation. The facility was completed in 1982 and became operational in 1983.

The NTF is a high-pressure, cryogenic, fan-driven, closed-circuit, pressurized wind tunnel. The circuit has a 15:1 contraction ratio and a 3.81 m (25 ft.) long, 2.5 m (8.2 ft.) square test section with filleted corners [2, 3]. The floor and ceiling of the test section have 6 slots each (6% open ratio) to prevent near-sonic flow choking effects. Test section configuration variables are top and bottom wall divergence, reentry flap angle, and initial diffuser angle [4]. When the test gas is air, the tunnel is cooled by water-fed coils located at the entrance to the settling chamber; when operating in cryogenic mode, the test gas is nitrogen and heat is removed by evaporating liquid nitrogen that is sprayed into the tunnel circuit upstream of the fan. During cryogenic testing, rapid model access with a minimum loss of nitrogen and time is facilitated through the use of a movable cylindrical enclosure conditioned for personnel access while the plenum and tunnel remain cold.

The test gas is driven through the tunnel circuit by a system consisting of two variable-speed induction motors, a two-speed gear box, a synchronous motor, and a fixed-pitch, single-stage fan with variable inlet guide vanes (IGVs). To achieve a desired compression ratio, the drive system can be operated at 1) a constant, synchronous fan speed where the IGVs are adjusted, or 2) a variable fan speed where the induction motors are used to drive the fan at a range of operational speeds.

Through different combinations of test gas, fan speed, IGV angle, and gear ratio, the airflow within the facility can be adjusted to match model size – true-flight aerodynamics can be duplicated for models as small as one-fiftieth the size of an actual aircraft. The NTF is capable of an absolute pressure range of 15 psi to 125 psi, a temperature range of -320°F to 150°F, a Mach number range from 0.1 to 1.2, and a Reynolds number (Re) range of 3×10^6 to 120×10^6 per foot. The NTF is depicted in Figure 2-1.
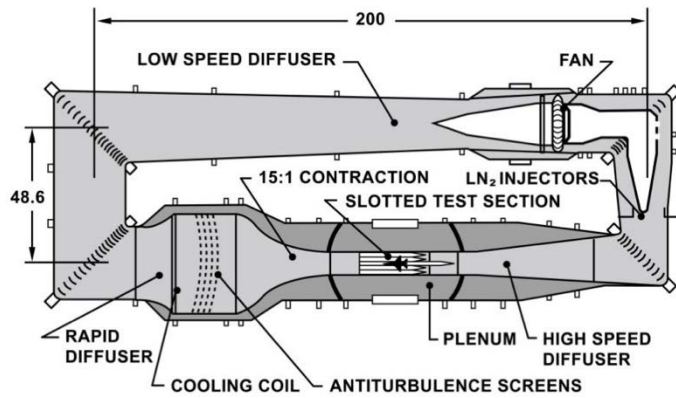
a) Aerial View   b) NTF circuit

Figure 2-1: The National Transonic Facility (NTF).

2.1 Geometry Development

The labor-intensive process to generate an accurate surface model of the NTF for grid generation purposes commenced with a laser scan of the facility to map the "as-built" geometry. This approach captures deviations from the construction drawings and changes in the structure that have occurred over time. The Geographic Information System (GIS) team at NASA LaRC scanned the surface of the tunnel circuit and plenum. The point-cloud data for the tunnel circuit contained over 251×10^6 points; the point-cloud data for the plenum contained approximately 205×10^6 points. A top view of the plenum data is given in Fig. 2-2a. Note the outline of the plenum, tunnel surfaces, model support arc, and plenum support structures. A close-up of the test section ceiling is presented in Fig. 2-2b. The slots, reentry flaps, and light sources are clearly discernible. The scanned data were given to the GEOLAB group at LaRC to process and convert into Computer Aided Design (CAD) surfaces for grid generation.

GEOLAB personnel toured the facility to understand its layout and features, and to generate a cache of photographs for reference. The laser-generated data were imported into the GeoMagic software program to sample various aspects of the point-cloud, remove extraneous data, and build the entire NTF geometry surface by surface. Fig. 2-2b shows a cross section of the point-cloud data for the test section and plenum. The data, in conjunction with photographs, construction drawings, and engineering judgment were used to create a geometric representation of the NTF tunnel in the Unigraphics CAD software program.

The Unigraphics CAD software program was used to properly construct the tunnel geometry. That geometry was then rechecked against the point data in GeoMagic and iteratively refined until it was considered satisfactory. The dimensions of the final CAD surfaces are very close to those of the construction drawings. For example, the test section has a width and height of 8.202 ft. and 8.222 ft., respectively, at its midpoint; the corresponding construction drawing dimensions at the same location are 8.202 ft. and 8.202 ft. The data also suggest that, for the test section walls, idealized planar surfaces are adequate to represent the as-built geometry.

The surfaces constructed in this manner capture additional details of the NTF tunnel that do not appear in the construction drawings. These details include small changes over time and slight mismatches between angles of the nonideal surfaces of many components. Not all of the details were included to make the geometry acceptable by current grid generation tools. The surfaces comprising the NTF high-speed leg were grouped into the components listed in Table 2-1. CAD renderings of these components are depicted in Figs. 2-3 and 2-4.
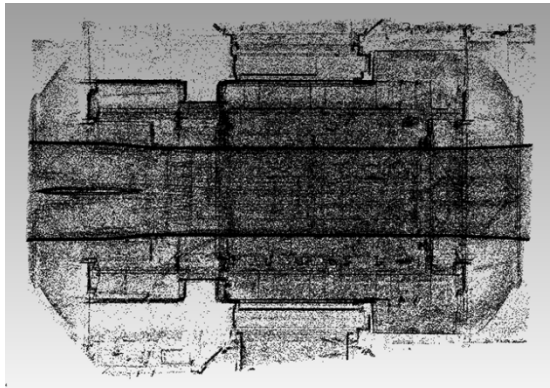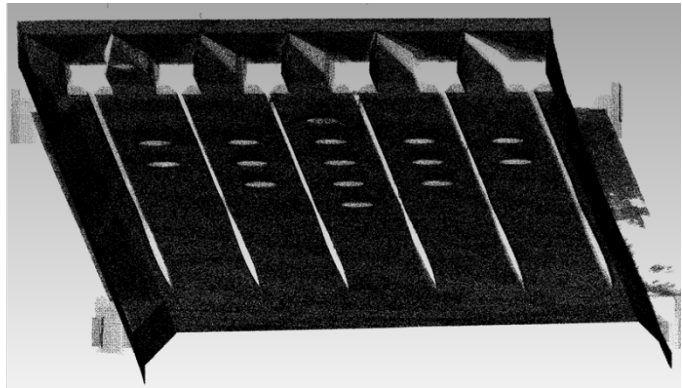
a) Top view   b) Test section ceiling

Figure 2-2: Point-cloud data for the NTF plenum.
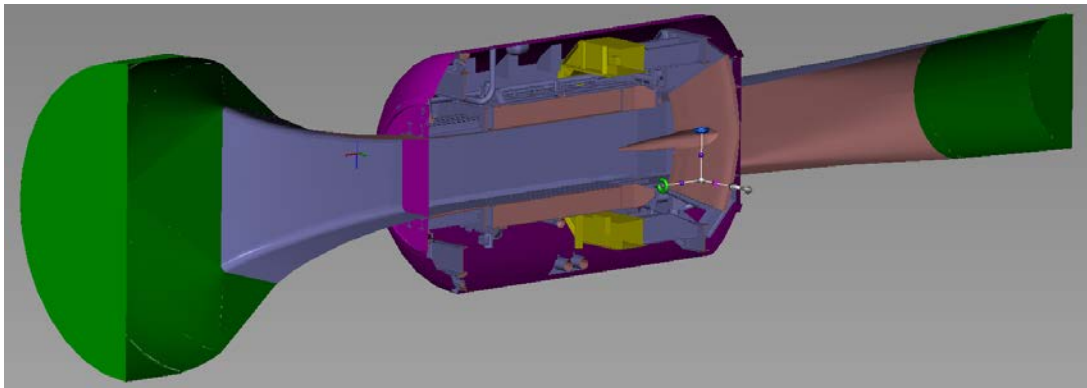
Figure 2-3: NTF high-speed leg (view at bisecting plane).
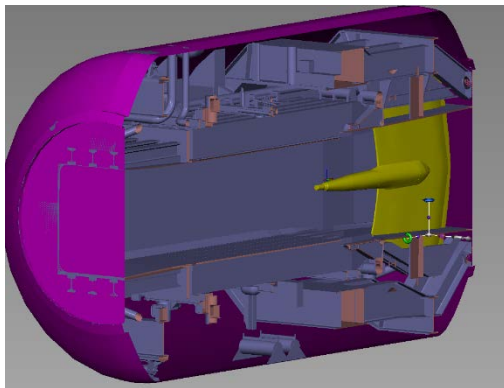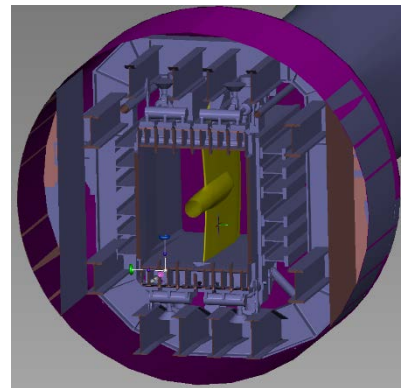
a) View looking downstream   b) Model support

Figure 2-4: NTF plenum volume definition.

Table 2-1. NTF high-speed leg components.

Component	Sub-assembly
1. Plenum shell	
2. Upstream plenum support (octagon 1)	
3. Midstream plenum support (octagon 2)	Plenum support
4. Downstream plenum support (octagon 3)	
5. Plenum wall protrusions	
6. Plenum I-beams and standing platforms	
7. Contraction to test section transition	
8. Test section walls	
9. Test section ceiling slots	
10. Test section ceiling reentry flaps	Test section
11. Test section floor slots	
12. Test section floor reentry flaps	
13. Test section side wall support	
14. Walls for model support section	
15. Test section movable reentry flaps (set at 0 degrees)	
16. Model support ceiling brackets	Model support
17. Model support floor brackets	
18. Model support seal area lower	
19. Model support arc and sting	
20. Leg components at plenum entrance and exit	Contraction/Diffuser
21. Leg components bounding high speed leg	

3.0 NUMERICAL MODELING APPROACH

The numerical characterization of the NTF commenced with high-fidelity simulations of the flow within the high-speed leg. Detailed geometry definitions for the elements that constitute this portion of the facility, developed from laser point-cloud scans of the "as-built" tunnel surfaces, were received from the GEOLAB and used for simulation with various CFD software programs.

3.1 Grid Generation

Three grid generation packages were investigated for creation of a suitable volume grid: VGRID, which is part of the NASA Langley Tetrahedral Unstructured Software System (TetrUSS) Computational Fluid Dynamics (CFD) software package [5]; Heldenmesh, by the Helden Aerospace Corporation [6]; and PowerFLOW®, by the EXA Corporation [7].

3.1.1 VGRID

Prior to grid generation, the "as-built" tunnel surfaces are read into GridTool (the geometry definition and setup component of TetrUSS) for generation of surface patches, assignment of boundary conditions, and determination of gridding parameters (sources). Despite inherent software limitations in the visualization of complex elements, construction of the NTF high-speed leg was completed after several months of painstaking effort. The components were then mated to form the test section, model support, plenum support, and contraction/diffuser subassemblies listed in Table 2-1 and depicted in Figure 3-1. A total of 8,175 surface patches were generated with GridTool to define the NTF high-speed leg.

All surfaces, including the plenum, were treated as viscous ($0.5 < y^+ < 1.0$). Cylindrical sources were used to discretize the volume defined by the wetted surfaces, and the volume between those surfaces and the plenum chamber reservoir. Judiciously placed line sources were also employed to improve definition of the model mounting system and certain ancillary components outside the main flow path. A total of 11,175 sources were distributed throughout the system.

a) Test section	b) Model support	c) Plenum support
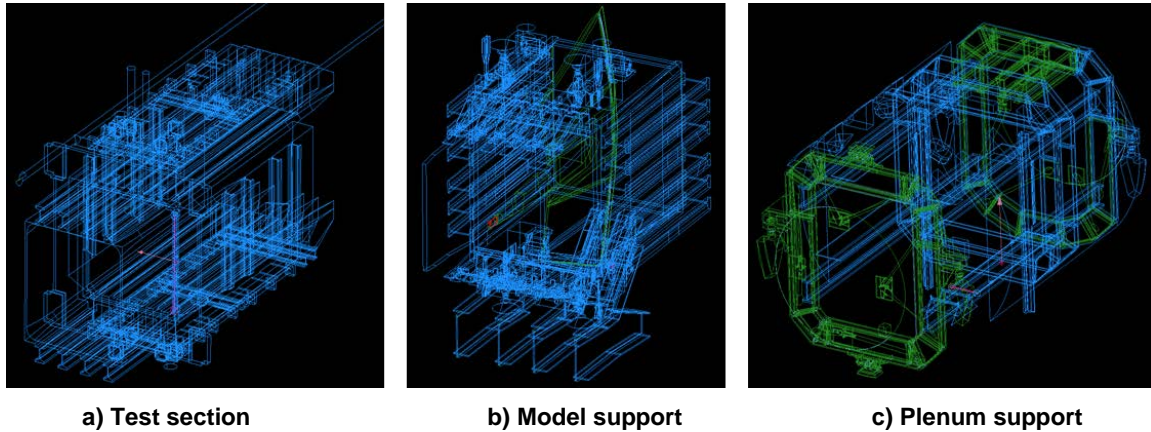
Figure 3-1: Structural subassemblies within plenum volume (GridTool).

Output from GridTool is read into VGRID (the unstructured grid generator within TetrUSS) to construct surface and volume meshes. Since VGRID was not designed to handle highly detailed geometries, generation of an adequate surface grid was problematic at best; a suitable, unstructured volume grid for simulation of the flow inside the high-speed leg could not be constructed despite numerous grid modifications and ancillary geometry simplifications. Thus, VGRID should not be used for the discretization of extremely complex geometries such as the NTF.

3.1.2 HELDENMESH

Heldenmesh is a software system developed by the Helden Aerospace Corporation for the rapid generation of high quality, three-dimensional, unstructured meshes about arbitrary complex configurations. The software was developed to streamline the application of CFD in a demanding production environment by transforming the mesh generation process from one currently measured in days-per-mesh to one measured in meshes-per-day. The Heldenmesh software system consists of two primary tools, Heldenpatch and Heldenmesh. The former is the interface between the underlying CAD geometry definition and the Heldenmesh grid generator, and includes geometry clean-up, management, and geometric transformation capabilities.

An important advantage of Heldenmesh is that the software can use GridTool input for mesh generation. Thus, the NTF surface patch assembly generated for VGRID was used to create a suitable volume grid after a few iterations. Heldenmesh-generated line sources, a refinement factor of 0.95, and a source growth factor of 0.3 were used to generate a coarse volume mesh for the empty tunnel. The mesh has approximately 150×10^6 tetrahedra and includes the model-mounting system. Depictions of the surface grid are presented in Fig. 3-2.

a) High-speed leg   b) Test section floor
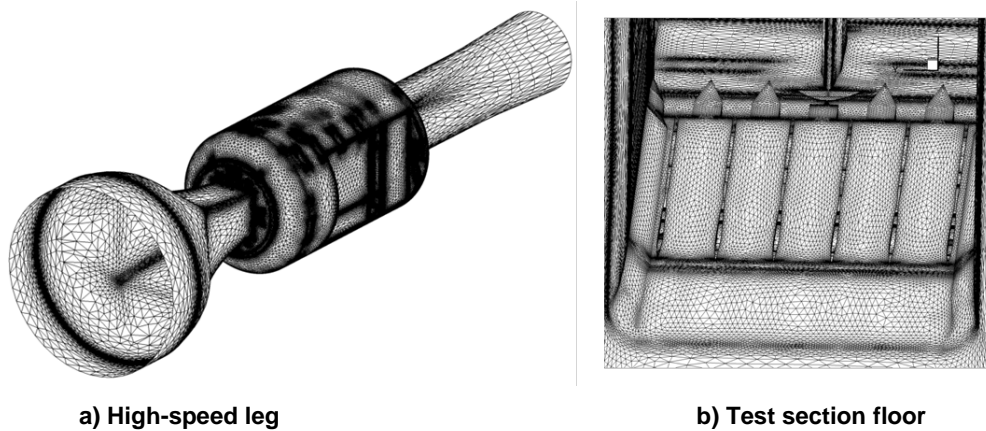
Figure 3-2: Surface grid of the empty NTF high-speed leg (Heldenmesh).

3.1.3 POWERFLOW®

PowerDELTA [8], the geometry preparation module of PowerFLOW®, maintains a parametric data structure very similar to that of traditional solid modelling CAD software and provides all the necessary tools to prepare CAD models for simulation – tessellation, remeshing, wrapping, and mesh editing tools. Surfaces defined in CAD-native formats are preferred because clean-up is minimal, but files in STEP and IGES formats are also accepted. Within PowerDELTA, extremely complex geometries can be easily organized into partitions with different meshing requirements. Output from PowerDELTA is used by PowerCASE [9] to create, edit, and compile a simulation case: grid spacing parameters, boundary conditions, and simulation time are specified with this tool. A Cartesian approach is followed during grid generation, supporting the efficient implementation of the lattice Boltzmann scheme used for flow simulation. To achieve local mesh refinement, regions of variable resolution (VR) can be applied that successively decrease voxel size by factors of two. The compiled case file controls construction of the mesh produced by the discretizer; thus, surface and volume mesh creation is automatic once the proper parameters have been defined. A suitable volume mesh for the high-speed leg can be constructed from IGES geometry files in a few days.

The NTF high-speed leg has three characteristic gap types that drive the minimum size of the Cartesian volume elements (voxels) in the grid: type 1, approximately 3 mm (0.12 in.) across, are located between the side walls of the upper/lower reentry flaps and their corresponding movable flaps (set at 0°); type 2, about 7 mm (0.275 in.) wide, reside between the model support section roof/floor and the arc; and type 3, approximately 9.4 mm (0.37 in.) wide, identify the minimum width (neck) of the slots in the roof/floor of the test section. A relatively coarse-resolution volume grid, where the gaps in the geometry were resolved with 2, 5, and 7 voxels for types 1, 2, and 3, respectively, was generated for the empty tunnel. The mesh contains approximately 397×10^6 voxels. All surfaces are viscous, except the settling chamber. For this component, inviscid surfaces were used to prevent formation of a boundary layer and thus partially simulate the effect of antiturbulence screens. Cross-sections of the volume mesh for the empty tunnel are presented in Fig. 3-3. Relatively coarse meshes were also generated for installations of a BoR and an early version of the NASA CRM. These meshes contain approximately 450×10^6 voxels and 540×10^6 voxels, respectively. For the latter, voxel size near the wing and nacelle surfaces is 0.1875 mm (0.00738 in.).

a) Plenum, y = 0   b) Model mounting system
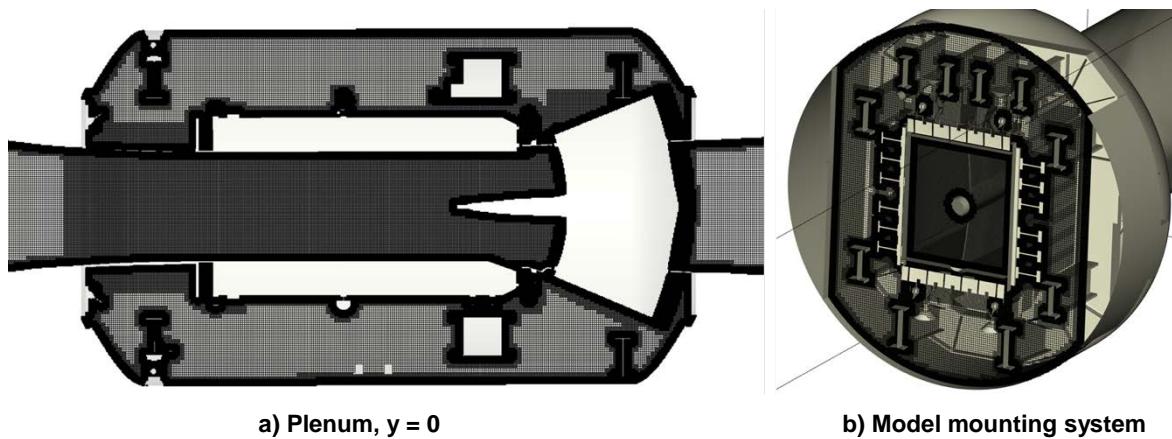
Figure 3-3: Volume grid of the empty NTF (PowerDELTA).

3.2 Flow Solver

Two flow solvers were used to characterize the flow within the NTF high-speed leg: USM3D, from the TetrUSS package, and PowerFLOW®.

3.2.1 USM3D

USM3D is a tetrahedral cell-centered, finite-volume Euler and Navier-Stokes (NS) flow solver. Inviscid flux quantities are computed across each cell face using Roe's flux difference splitting [10]. Spatial discretization is accomplished by a reconstruction process based on an analytical formulation for computing solution gradients within tetrahedral cells [11]. The solution is advanced to a steady-state condition by an implicit backward-Euler time-stepping scheme [12]. Flow turbulence effects are modeled by 1) the Spalart-Allmaras (SA) one-equation model [13] coupled with a wall function to reduce the number of cells in the sublayer region of the boundary layer, and 2) by a modified k-ε two-equation model [14]. USM3D has been parallelized for efficient operation on both shared and distributed memory computer systems.

USM3D supports the standard boundary conditions of flow tangency or no-slip on solid surfaces, characteristic inflow/outflow for subsonic boundaries, and freestream inflow and extrapolation outflow for supersonic flows. The solver also features boundary conditions for wake flow, jet engines, and propellers.

3.2.2 PowerFLOW®

PowerFLOW® solves unsteady subsonic, transonic, and supersonic flows through extensions of the lattice Boltzmann method (LBM) that track the motion of macromolecules through space and time [15-20]. The approach inherently conserves mass, momentum, and energy to capture fluid behavior precisely. At a macroscopic level, LBM uses a simpler and more general physics formulation than methods based on the NS equations. Recovery of the macroscopic hydrodynamics of the NS equations through use of the LBM equations is accomplished through the Chapman-Enskog expansion [21,22]. The flow solver has been extensively validated for a wide variety of applications ranging from academic direct numerical simulation (DNS) cases to industrial flow problems in the fields of aerodynamics and aeroacoustics [23,24]. Until recently, PowerFLOW® had been restricted to the low compressible isothermal flow regime. Developments based on the research documented in Refs. 25 and 26 have enabled extension of the local Mach number up to about 2.0 [27]. This includes the ability to resolve shock discontinuities and to model consistent compressible gas dynamics while retaining benefits of the LBM, such as a highly efficient implementation suitable for computations on thousands of processors.

Without any turbulence modelling, the LBM flow simulation is identical to a DNS of the flow. For flows with a high Re, the lattice Boltzmann Very Large Eddy Simulation (LB-VLES) approach is used to reduce computational resource requirements [15,28]. This means that turbulence is modelled in areas of attached flow such as boundary layers but resolved in wakes or regions of detached flows [23,29].

The lattice Boltzmann bounce-back boundary condition for no-slip, or the specular reflection for free-slip condition, are established by way of a volumetric formulation [15,16] near the wall for randomly oriented surface elements (surfels) within the voxels. This formulation of the boundary condition on a curved surface intersecting the Cartesian grid is by nature mass-, momentum-, and energy-conservative while preserving the spatial order of accuracy of the underlying LBM numerical scheme. To reduce the near-wall resolution requirements for high Re flows, a hybrid wall function is used to model the region of the boundary layer closest to the solid surfaces [23,30] including compressibility and pressure gradient effects.

4.0 RESULTS

The numerical characterization of wind tunnel flows requires the specification of a boundary condition to drive the test gas. For the NTF high-speed leg simulations, the only parameters available were total pressure ($P_{t,in}$) and total temperature ($T_{t,in}$) at the settling chamber inlet, test section Mach number (M_T), and unit Reynolds number (Re/ft). Thus, it was necessary to determine, iteratively, a suitable value for the static pressure at the diffuser exit ($P_{s,out}$) that would yield a sufficiently converged solution for the desired M_T. An initial guess for $P_{s,out}$ was obtained from streamtube area relationships for isentropic flows. Preliminary, time-accurate simulations have been generated for three configurations: empty tunnel, BoR installed, and CRM installed. Target airflow input variables and number of cores used for the simulations are listed in Table 4-1. USM3D calculations were performed in the NASA NAS Pleiades supercomputer; cases using PowerFLOW® were executed in the NASA LaRC mid-level computer cluster, K.

Table 4-1. NTF high-speed leg simulation characteristics.

Case	$P_{t,in}$, psia	$T_{t,in}$, °F	M_T	Re/ft, ×10^6	Cores used	
					USM3D	PowerFLOW®
Empty tunnel	33.80	120	0.70	8.0	1024	-
	31.37	120	0.80	8.0	-	512
BoR installed	30.50	120	0.85	8.0	-	400
CRM installed	30.50	120	0.85	8.0	-	512

4.1 Empty Tunnel

Overall flow behavior inside the NTF high-speed leg at $M_T = 0.7$ is depicted in Fig. 4-1, which shows instantaneous Mach number contours at two planes bisecting the configuration. The results were obtained with USM3D; the SA one-equation model was used to simulate turbulence effects. Note from the figure that 1) flow entrainment has been established in the reentry flap area; and 2) a region of momentum deficit, present near the diffuser walls, develops into flow separation as the flow expands toward the exit of the diffuser.

The flow inside the tunnel, sampled at two axial locations, is presented in Fig. 4-2. Note from Fig. 4-2a that, at the test section center x = 3.81 m (12.5 ft.), flow entrainment into the plenum through the slots is well established, quickly expanding into the channels above and below the test section. At a plane intersecting the movable reentry flaps (Fig. 4-2b), the transfer of mass into the plenum is more vigorous. A region of momentum deficit caused by the wake emanating from the mounting sting is visible near the trailing edge of the arc (Fig. 4-2c).
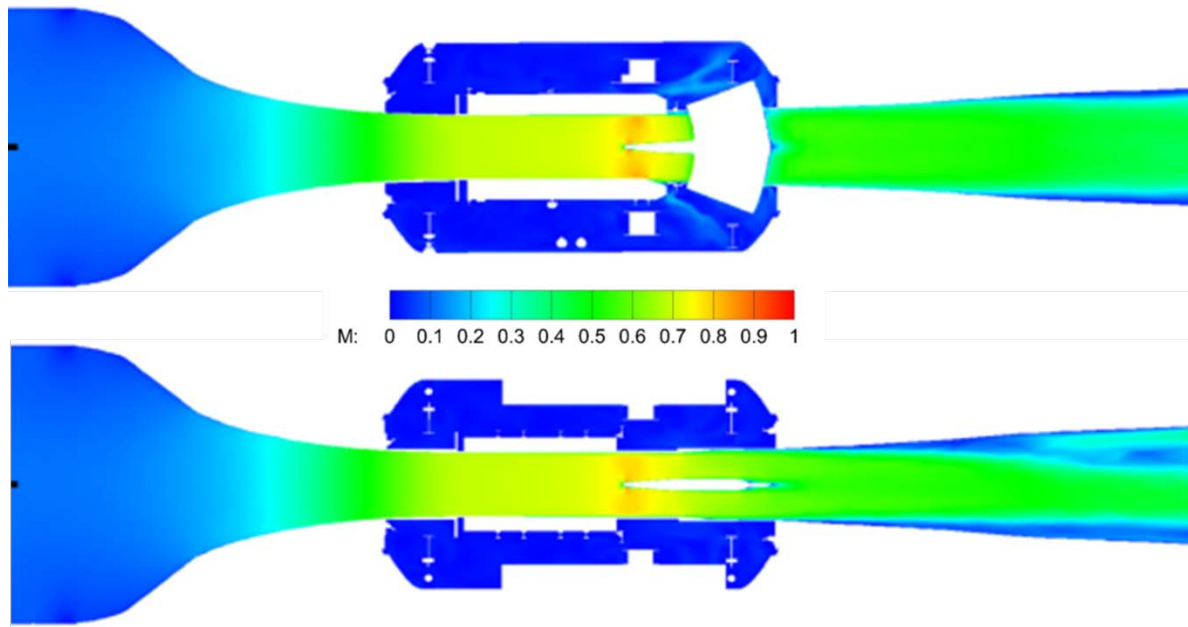
Figure 4-1: Instantaneous flow, $M_T = 0.7$ (USM3D). Top image: y = 0 plane; bottom image: z = 0 plane.

| a) x = 12.5 ft. | b) x = 25 ft. | c) x = 35 ft. |
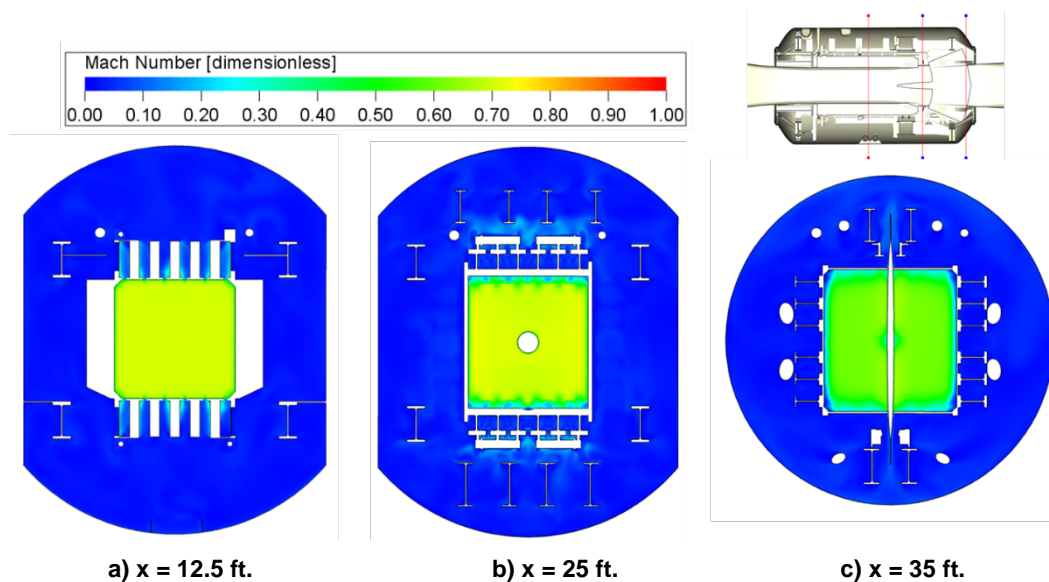
Figure 4-2: Instantaneous flow at various x locations, $M_T = 0.7$ (USM3D).

Results from PowerFLOW® simulations at $M_T = 0.806$ are presented in Fig. 4-3, which shows instantaneous Mach number contours at two planes bisecting the mounting sting. The general flow trends are similar to those observed for $M_T = 0.7$. However, the increase in momentum gives rise to transonic flow behavior (shock formation) in the vicinity of the blunt-faced, empty model mounting structure.

Flow entrainment through the slots is well established, as seen in Fig. 4-4a. Mass transfer into the plenum increases in the reentry flap area (Fig. 4-4b), especially through a large gap in the floor necessary to accommodate flap displacement, which is located slightly upstream of the mounting arc (see Fig. 4-5a). The wakes of the sting and

reentry flaps are clearly visible near the trailing edge of the arc (Fig. 4-4c); substantial flow leakage through the type 2 gaps at this station is also observed. At a location within the diffuser (Fig. 4-4d), the flow appears to be separated from most of the perimeter. By the time it reaches the exit, the flow is almost jet-like in nature. The causes of this behavior are physical; however, the flow features are also affected by computational circumstances.

Secondary flows driven by Reynolds-stress gradients always form at the vertices of long ducts of non-circular cross-section, even if the vertices or corners have been filleted. These vortical structures have magnitudes usually less than 1.5% of the bulk flow velocity [31]. The flow entering the diffuser is also characterized by a thick boundary layer and non-uniform velocity profiles caused by the wakes from the model support apparatus and the reentry flaps. Examination of the geometry indicates that the as-built, high-speed diffuser is composed of two sections: a rectangular-to-circular transition with half-angle $\theta \sim 6°$ for approximately 65% of its length (depicted by the red line in the tunnel sketch at top right of Fig. 4-4) and $\theta \sim 15.5°$ for the remaining 35% (green line), and a conical diffuser with $\theta \sim 7.5°$ (purple line). Thus, each section can be considered as a wide-angle diffuser ($2\theta > \sim 8°$) with a rapid increase in cross-sectional area. The highly non-uniform nature of the incoming flow, combined with the adverse pressure gradient encountered in the diffuser, suggest that boundary layer control may be the only way to avoid separation [32, 33].

The results presented here correspond to meshes with relatively low spatial resolution. Although its features will be better defined for denser grids, the macroscopic aspects of the flow through the NTF high-speed leg are expected to change little with improved resolution. Of greater importance to the quality of the flow entering the test section would be factors, such as flow angularity and asymmetric pressure distribution, that result from considering the entire circuit [34].
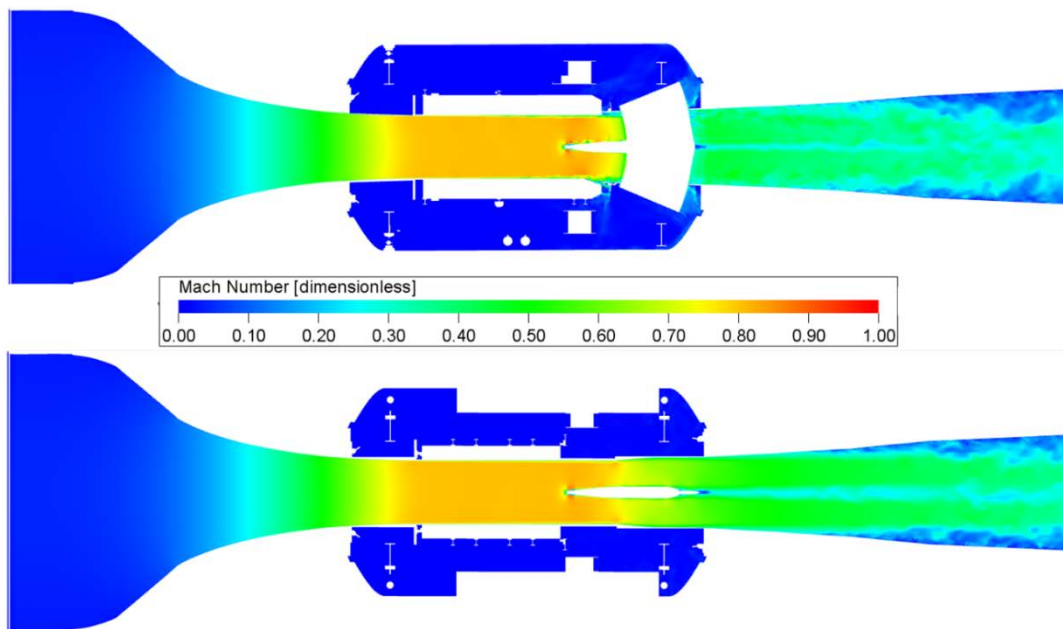
Figure 4-3: Instantaneous flow, $M_T = 0.806$ (PowerFLOW®). Top image: y = 0 plane; bottom image: z = 0 plane.

a) x = 12.5 ft.   b) x = 25 ft.   c) x = 35 ft.   d) x = 74 ft.
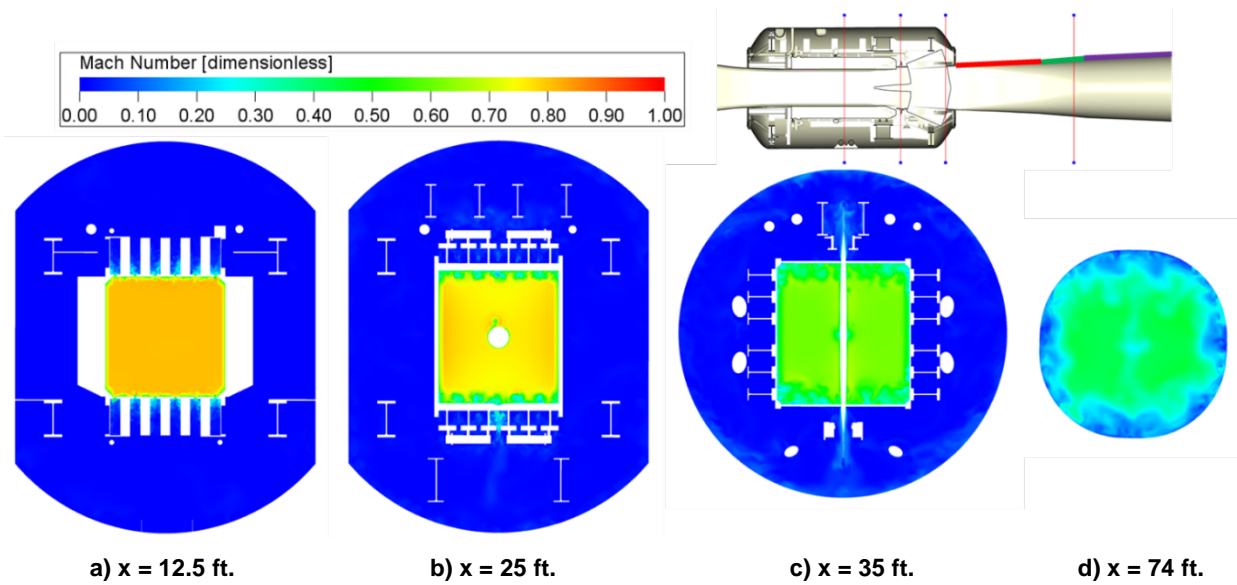
Figure 4-4: Instantaneous flow at various x locations, M_T = 0.806 (PowerFLOW®).

a) Floor (view looking downstream)   b) Ceiling (view looking upstream)
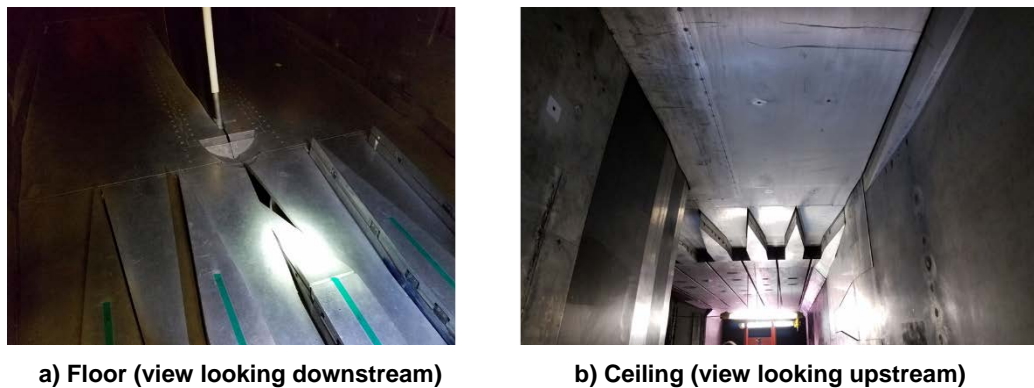
Figure 4-5: Movable reentry flaps, NTF test section.

4.2 Body of Revolution Installed

The advent of supercritical design concepts in the 1960s fostered the development of transonic aircraft and emphasized the importance of accurate drag measurements in near-sonic conditions. Experimental studies to evaluate the severity of wind-tunnel wall interference effects were undertaken by NASA in the early 1970s. One such investigation [35], which used geometrically similar bodies of revolution as test articles, revealed that significant errors in model drag coefficients at transonic speeds existed for test-section blockage ratios that were an order of magnitude below the previously considered safe value. An expanded version of that experiment was conducted in 2005 at the NTF [36]. The test articles were scaled up to maintain the same blockage ratios encountered in the earlier investigation. The largest model, the C4 BoR (L = 1.74 m or 68.53 in.; D_{max} = 0.1843 m or 7.2554 in.) was chosen for the present study. The test article, installed at angle of attack $\alpha = 0°$, is depicted in Fig. 4-6.

Overall flow behavior from PowerFLOW® simulations at M_T = 0.854 is depicted in Fig. 4-7, which shows instantaneous Mach number contours at two planes bisecting the configuration. Note from the figure that transonic

flow effects are present within the entire test section: a weak shock forms over most of the test article surface area and stronger shocks are generated at the surface discontinuities of the mounting sting. Also observe that separation of the flow inside the diffuser appears to be asymmetric and more extensive toward the top and bottom walls; jet flow develops early, within the first section of the wide-angle rectangular-to-circular transition.

a) NTF test section   **b) CAD model**
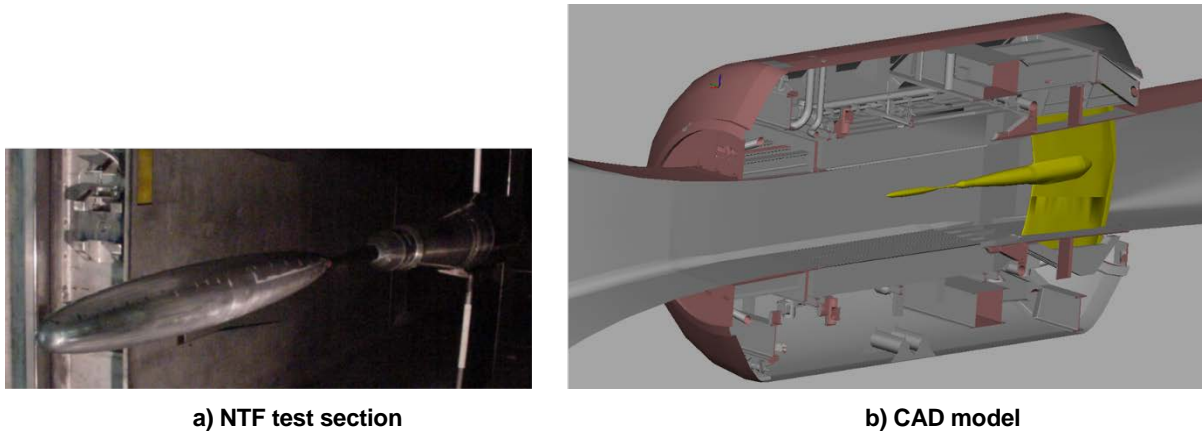
Figure 4-6: Installed C4 body of revolution.
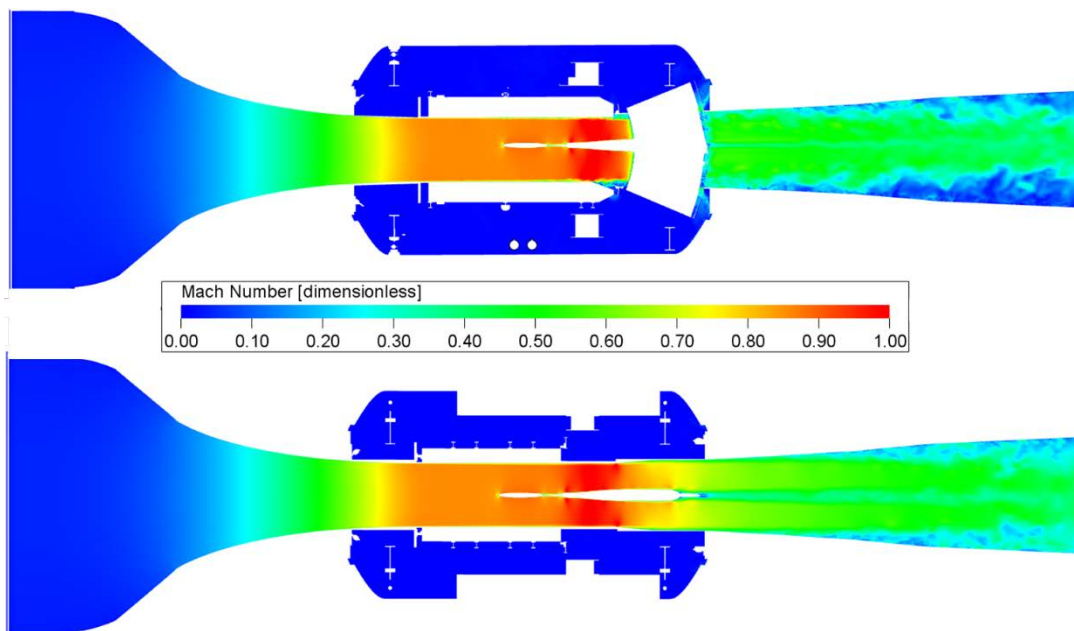
Figure 4-7: Instantaneous flow, M$_T$ = 0.854 (PowerFLOW®). Top image: y = -0.083 ft. plane; bottom image: z = 0.52 ft. plane.

4.3 Common Research Model Installed

To answer numerous requests for the development of experimental data bases to validate current and next-generation CFD software, NASA designed an open research configuration based on a conventional transonic aircraft. Design point conditions were $M_\infty = 0.85$, nominal lift $C_L = 0.5$, and $Re = 40 \times 10^6$ per reference chord [37]. This configuration, the CRM, has a wing aspect ratio $AR = 9.0$, a taper ratio $\lambda = 0.275$, and a span (b) sized for

integration into a fuselage that is representative of commercial widebody transports. The CAD model used in this study (L = 1.693 m or 66.65 in.; b = 1.587 m or 62.48 in.) incorporates aeroelastic wing deflections encountered at the nominal cruise condition. An early version of the CRM, installed at $\alpha = 0°$, is depicted in Fig. 4-8.

Instantaneous Mach number contours from PowerFLOW® simulations at $M_T = 0.851$ are presented in Fig. 4-9 for two perpendicular planes passing through the nose of the CRM fuselage. Note from the figure that weak shocks develop at various locations on the fuselage and mounting apparatus. Asymmetric jet flow results from early separation within the high-speed diffuser.

a) NTF test section   b) CAD model
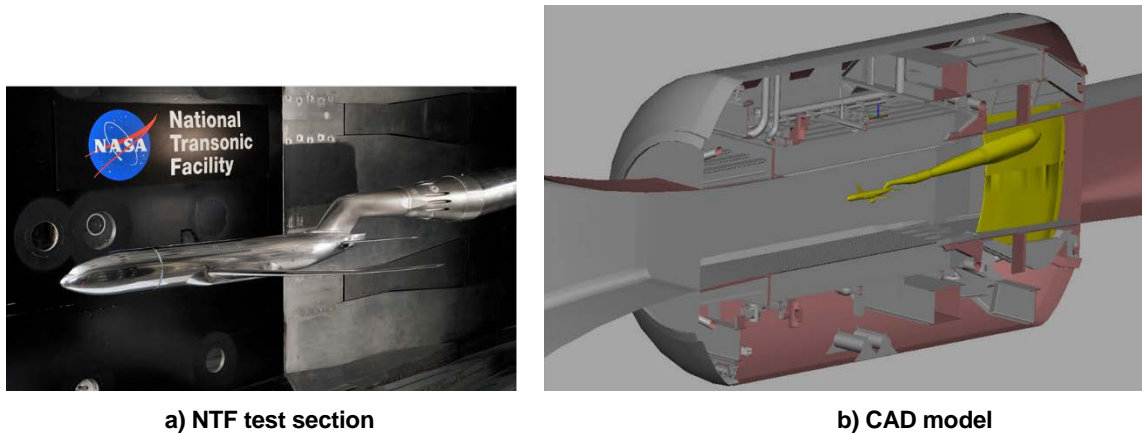
Figure 4-8: Installed NASA Common Research Model.
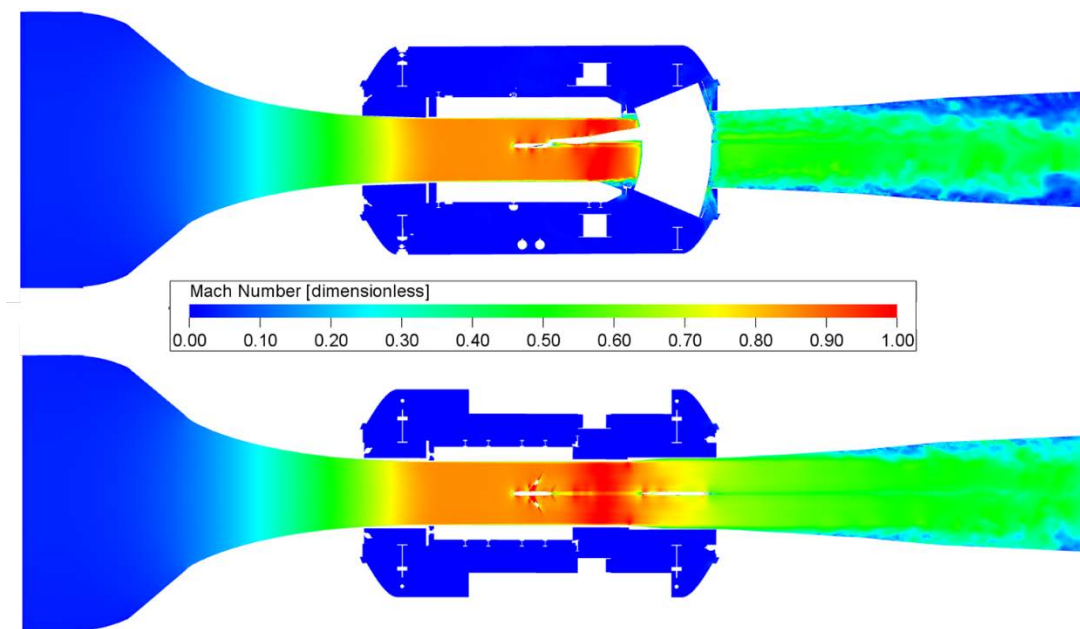
Figure 4-9: Instantaneous flow, $M_T = 0.851$ (PowerFLOW®). Top image: y = -0.083 ft. plane; bottom image: z = 0.45 ft. plane.

A better assessment of transonic flow effects on the three configurations can be reached by considering Fig. 4-10, which depicts contours of instantaneous Mach number (left side) and nondimensional density (right side) within

the test section. Observe from the top row of images that, as expected, the blunt face of the empty mounting sting causes the flow to separate and convect as vortices over the top surface of the sting. Vortical flow does not develop on the bottom surface. This asymmetry is caused by the geometry of the reentry flap system: a large gap on the floor of the test section (see Fig. 4-5a) releases pressure in that region, preventing the formation of vortices. The reentry flaps on the test section ceiling, however, are uniform and devoid of large openings (see Fig. 4-5b). A weak shock system, clearly visible in the density plot, forms at the face of the sting. Shock-shear layer interaction [38] is also present in this region. Transonic flow behaviour for the C4 BoR is depicted in the mid-row images. Observe that a well-defined shock develops over most of the model surface. Note also that compression and expansion of the flow as it negotiates the surface slope discontinuities of the mounting apparatus cause shocks to form over that component as well. The characteristics of the flow over the CRM are depicted on the bottom row of images. At least three shock systems are present on the fuselage surface, and various others develop over the highly discontinuous surface of the mounting sting. The wake of the fuselage is also visible in the Mach number contours.
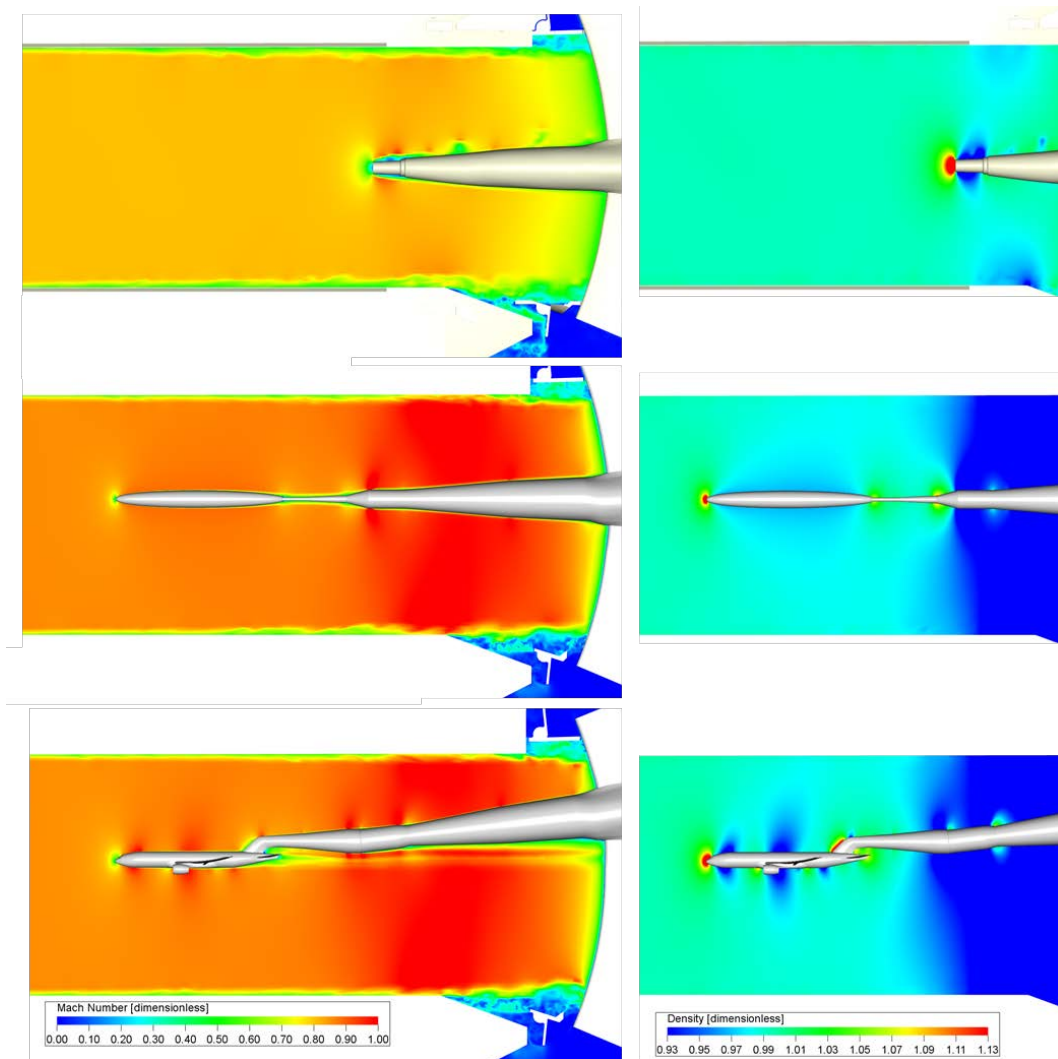
Figure 4-10: Instantaneous Mach number and density contours within the test section (PowerFLOW®). Top row: empty tunnel (M_T = 0.806); middle row: C4 BoR installed (M_T = 0.854); bottom row: NASA CRM installed (M_T = 0.851).

5.0 CONCLUDING REMARKS

Ongoing efforts to characterize the NTF flow physics were summarized in this paper. The process of modelling the wind tunnel, including all the important geometric complexities of the facility, was presented. The difficulties that were experienced due to the level of detail required to adequately model the NTF have been described and the conclusion drawn that VGRID is inadequate to generate volume grids of this nature. Preliminary, time-accurate results for three configurations – empty tunnel, BoR installed, and CRM installed – show that CFD predicts the flow as expected at transonic speeds. Weak shock formation over the test articles and model mounting apparatus was observed, as was conspicuous flow separation within the high-speed diffuser.

6.0 REFERENCES

[1]   https://crgis.ndc.nasa.gov/historic/National_Transonic_Facility, cited January 16, 2018.

[2]   Chan, D. T., Milholen, W. E., Jones, G. S., and Goodliff, S. L., "Thrust Removal Methodology for the FAST-MAC Circulation Control Model Tested in the National Transonic Facility," AIAA 2014-2402, 2014.

[3]   Bobbitt, Jr., C., and Everhart, J., "Status of the National Transonic Facility Characterization," AIAA 2001-0755, 2001.

[4]   Foster, J. M., and Adcock, J. B., "User's Guide for the National Transonic Facility Research Data System," NASA TM-110242, April 1996.

[5]   Frink, N. T., Pirzadeh, S. Z., Parikh, P. C., Pandya, M. J., and Bhat, M., "The NASA Tetrahedral Unstructured Software System (TetrUSS)," *The Aeronautical Journal*, Vol. 104, No. 1040, October 2000, pp. 491–499.

[6]   Heldenmesh Users' Manual, Version 1.1, Helden Aerospace Corporation, November 2016.

[7]   http://exa.com/en/product/simulation-tools/powerflow-cfd-simulation, cited January 18, 2018.

[8]   PowerDELTA User's Guide, Release 2.5, Revision 1, 2016.

[9]   PowerCASE User's Guide, Release 5.4, Revision 1, 2017.

[10]   Roe, P., "Characteristic based schemes for the Euler equations," *Annual Review of Fluid Mechanics*, Vol. 18, 1986, pp. 337–365.

[11]   Frink, N., "Recent Progress Toward a Three-Dimensional Unstructured Navier-Stokes Flow Solver," AIAA 94-0061, January 1994.

[12]   Anderson, W. and Bonhaus, D., "An implicit upwind algorithm for computing turbulent flows on unstructured grids," *Computers Fluids*, Vol. 23, No. 1, 1994, pp. 1–21.

[13]   Spalart, P. and Allmaras, S., "A one-equation turbulence model for aerodynamic flows," AIAA 92-0439, January 1992.

[14]   Wang, Q., Massey, S. J., and Abdol-Hamid, K. S., "Implementation of Advanced Two-Equation Turbulence Models in the USM3D Unstructured Flow Solver," NASA CR-2000-210102, April 2000.

[15]   Chen, H., "Volumetric Formulation of the Lattice-Boltzmann Method for Fluid Dynamics: Basic Concept," *Physical Review E*, Vol. 58, No. 3, 1998, pp. 3955–3963, doi: dx.doi.org/10.1103/PhysRevE.58.3955.

[16] Chen, H., Texeira, C., and Molvig, K., "Realization of Fluid Boundary Condition via Discrete Boltzmann Dynamics," *Int. Journal of Modern Physics C*, 1998, pp. 1281–1292, doi: 10.1142/S0129183198001151.

[17] Chen, H., Kandasamy, S., Orszag, S., Shock, R., Succi, S., and Yakhot, V., "Extended Boltzmann Kinetic Equation for Turbulent Flows," *Science*, No. 301, 2003, pp. 633–636.

[18] Chen, S., and Doolen, G., "Lattice Boltzmann Method for Fluid Flows," *Annual Review of Fluid Mechanics*, Vol. 30, 1998, pp. 329–364.

[19] Shan, X., Yuan, X.-F. and Chen, H. "Kinetic theory representation of hydrodynamics: a way beyond the Navier Stokes equation", *Journal of Fluid Mechanics*, Vol. 550, 2006, pp. 413–441.

[20] Zhang, R., Shan, X. and Chen, H. "Efficient kinetic method for fluid simulation beyond the Navier-Stokes equation," *Physical Review E, American Physical Society*, Vol. 74, No. 4, October 2006, doi: doi.org/10.1103/PhysRevE.74.046703.

[21] Chen, H., Chen, S., and Matthaeus, W. H., "Recovery of the Navier-Stokes equations using a lattice gas Boltzmann method," *Physical Review A*, Vol. 45, No. 8, April 1992, pp. R5339-R5342, doi: dx.doi.org/10.1103/PhysRevA.45.R5339.

[22] Qian, Y. H., D'Humières, D., and Lallemand, P., "Lattice BGK Models for Navier-Stokes Equation," *Europhysics Letters*, Vol. 17, 1992, pp. 479–484, doi:10.1209/0295-5075/17/6/001.

[23] Fares, E. and Noelting, S., "Unsteady Flow Simulation of a High-Lift configuration using Lattice-Boltzmann Approach," AIAA paper 2011-869, 2011.

[24] Khorrami, M. R., Fares, E., and Casalino, D., "Towards Full-Aircraft Airframe Noise Prediction: Lattice-Boltzmann Simulations," AIAA paper 2014-2481, June 2014.

[25] Chen, H., Goldhirsch, I., and Orszag, S. A., "Discrete Rotational Symmetry, Moment Isotropy, and Higher Order Lattice Boltzmann Models," *Journal of Scientific Computing*, Vol. 34, No. 1, 2008, pp. 87–112.

[26] Chen, H. and Shan, X., "Fundamental conditions for N-th-order accurate lattice Boltzmann models," *Physica D: Nonlinear Phenomena*, Vol. 237, No. 14-17, August 2008, pp. 2003–2008.

[27] Fares, E., Wessels, M., Li, Y., Gopalakrishnan, P., Zhang, R., Sun, C., Gopalaswamy, N., Roberts, P., Hoch, J., and Chen, H., "Validation of a Lattice-Boltzmann Approach for Transonic and Supersonic Flow Simulations," AIAA paper 2014-0952, 2014.

[28] Yakhot, V. and Orszag, S., "Renormalization Group Analysis of Turbulence," *Journal of Scientific Computing*, Vol. 1, No. 2, 1986, pp. 3–51, doi: 10.1007/BF01061452.

[29] Khorrami, M., Mineck, R., Yao, C., and Jenkins, N., "A Comparative Study of Simulated and Measured Gear-Flap Flow Interaction," AIAA paper 2015-2989, 2015.

[30] Fares, E., "Unsteady Flow Simulation of the Ahmed Reference Body using a Lattice Boltzmann Approach," *Journal of Computers and Fluids*, No. 35, 2006, pp. 940–950.

[31] Taylor, A. M. K. P., Whitelaw, J. H., and Yianneskis, M., "Turbulent Flow in a Square-to-Round Transition," NACA Contractor Report 3447, July 1981.

[32] Schubauer, G. B. and Spangenberg, W. G., "Effects of Screens in Wide-Angle Diffusers," NACA Report 949, June 1947.

[33] Mehta, R. D., "The Design of Wide-Angle Diffusers," Imperial College Aero Report 76-03, June 1976.

[34] Nayani, S. N., Sellers, W. L., Tinetti, A. F., Brynildsen, S. E., and Walker, E. L., "Numerical Simulation of a Complete Low-Speed Wind Tunnel Circuit," AIAA paper 2016-2111, January 2016.

[35] Couch, L. M. and Brooks, Jr., C. W., "Effect of Blockage Ratio on Drag and Pressure Distributions for Bodies of Revolution at Transonic Speeds," NASA TN D-7331, November 1973.

[36] Walker, E. L., "Statistical Calibration and Validation of a Homogeneous Ventilated Wall-Interference Correction Method for the National Transonic Facility," NASA TP-2005-213947, December 2005.

[37] https://commonresearchmodel.larc.nasa.gov/, cited March 10, 2018.

[38] Mehta, R. C., "Unsteady Flowfield Characteristics Over Blunt Bodies at High Speed," Chapter 5, Computational and Numerical Simulations, published by IntechOpen.